H^+ emission under room temperature and non-vacuum atmosphere from a sol-gel-derived nanoporous emitter

Yusuke Daiko[1,*], Satoshi Mizutani[1], Kodai Machida[2], Hiroaki Imataka[2], Sawao Honda[1] and Yuji Iwamoto

[1]*Department of Life Science and Applied Chemistry, Nagoya Institute of Technology, Gokiso-cho, Showa-ku, Nagoya, Aichi 466-8555, Japan.*

[2]*Department of Material Science and Chemistry, Graduate School of Engineering, University of Hyogo, Himeji, 671-2201, Japan*

[*]Corresponding author: Fax: +81 52 735-5281, Email: daiko.yusuke@nitech.ac.jp

Abstract

A high proton conducting P_2O_5-SiO_2 nanoporous glass-rod was prepared via sol-gel technique, and its tip was sharpened by a meniscus-etching method. The glass-rod shows proton conductivity of 1×10^{-3} at room temperature after absorption of water molecules. A palm-sized proton gun was prepared by utilizing the glass-rod as a H^+ emitter. A high voltage (~2.5 kV) was applied between the tip of glass-rod

and an extraction electrode, and a high ionic current was successfully observed even under non-vacuum atmosphere at room temperature. Protonation reaction for polyaniline was confirmed from the structural changes of C=N in quinone to protonated C-N^+. New applications of proton implantation will be expected especially in bioscience and medical technology.

Keyword: proton conduction, ion emission, mesoporous, meniscus-etching

1. Introduction

Ion implantation is one effective method for surface modification of materials, and has been applied for various field including semiconductor industry and bio-technology [1-4]. For example, proton (H^+) implantation, so-called proton therapy, has recently used most often in the treatment of cancer, in which an accelerated protons are irradiated directly to cancer cells [5]. In general, discharge plasma (gas) or liquid (e.g. liquid gallium (Ga) focused ion beam (FIB)) has been utilized for an ion source. However, in these cases, side reactions (generation of radicals or various ions with different mass such as H_2^+ and H_3^+

etc.) are unavoidable. Also, ion (particle) accelerators are huge and expensive. On the other hand, ion emission from solid electrolytes such as YSZ (yttria stabilized zirconia) has also been considered [6,7]. Hosono *et al.* showed that O^- ions exist inside cages of $12CaO \cdot 7Al_2O_3$ (C12A7) crystal (electrolyte), and they successfully observed O^- ion beam from the C12A7 by applying a high voltage [8,9]. In the case of these ion emissions from solid electrolyte, one crucial aspect is its high ion conductivity, and ion emission current increases with increasing ion conductivity of electrolyte [8]. Compared with gas and liquid ion sources, ion emission mechanism of such solid-emitter is simple and almost ~100% of emitted ions are O^- ion in the case for C12A7. Even through, a high vacuum (10^{-5} Pa or less) condition is usually required, and applications of ion implantations are thus still limited.

We have studied ion emissions from various types of ion conducting glasses, and H^+ emission utilizing nano-sharpening H^+ conducing glass-fiber was reported previously [10]. The glass-fiber was prepared via melt-quenching technique. The glass transition temperature (Tg) of the glass was around 400°C, and H^+ emissions were observed above Tg. Likewise the above-mentioned O^- emission, however, a high vacuum was necessary for H^+ emission by using the melt-quenched glass-fiber. We anticipate that an ion emission gun operating under room temperature and non-vacuum atmosphere, if developed, would open a new medical technology in which H^+ can be directly implanted into body tissues and cells in-air very easily. For this purpose, a solid electrolyte with high proton conductivity at room temperature is indispensable.

Nogami and Daiko reported that sol-gel-derived P_2O_5-SiO_2 porous glasses show high proton conductivity of ~10^{-2} S/cm at room temperature after absorption of water [11-13]. In this paper, we report

H^+ emission under room temperature and non-vacuum condition for the first time using the porous glass as a H^+ emitter. The evidence of H^+ emission was confirmed from a protonation reaction of polyaniline (from emeraldine base to emeraldine salt) based on Raman spectroscopy.

2. Experimental

$5P_2O_5$-$95SiO_2$ (mol%) glass was prepared by the sol-gel method using $Si(OC_2H_5)_4$ and $PO(OCH_3)_3$. $Si(OC_2H_5)_4$ (6 mL) was hydrolyzed with a mixed solution of C_2H_5OH and H_2O (as 0.15N-HCl aq) in molar ratios of 1:1 per mol of $Si(OC_2H_5)_4$. After the solution was stirred for 30 min, $PO(OCH_3)_3$ was added, followed by stirring for 1h. The resultant solution was further hydrolyzed by adding 4 mol H_2O (as 0.15N-NH_3 aq) per mol of $Si(OC_2H_5)_4$. After the hydrolyzing, 0.3mL of *N,N*-dimethylformamide (DMF) was added to the solution in order to prevent the generation of cracks during the following dry-processes.

The obtained solution was clear and poured into a conic-shaped container (1 mL), and then dried as follow: left the container at 35°C for 12 h, and then temperature was increased slowly from 35°C to 80°C (heating rate: 1°C/h) and kept at 80°C for 120 h. In order to hydrolyze the alkoxide completely, the obtained stiff gel was heated in a sealed vessel together with water at 120°C for 72 h (water vapor treatment), followed by heating in air at 700°C. The heating rate from room temperature to 700°C was 20°C/h, and held at 700°C for 5 h. Blackening (carbonization) of glass was seen after heating at 700°C without the water vapor treatment at 120°C.

For the sharpening of the glass, a meniscus-etching using HF solution and cyclohexane was

performed. Fig. 1 shows the schematic illustration of the meniscus-etching. After the etching, glass-rod was rinsed using distilled water and dried at 100°C for 30 h under vacuum (~10 Pa) in order to remove the absorbed cyclohexane completely.

Fig. 2 shows the setup of the H^+ conductivity and H^+ emission measurements. Proton conductivity was calculated from Cole-Cole plot by an AC impedance measurement using an LCR meter with frequencies ranging from 100 kHz to 20 Hz (ZM2375, NF corporation, Japan). Ag past was used for electrodes of the impedance measurement. For the H^+ emission measurement, a high voltage was applied using direct current (DC) power supply (HAR30P-10, Matsusada Precision, Japan) between Pt/C and extracted electrodes. Humidified 4%H_2-96%Ar gas was supplied into the cell using a bubbler. An anode reaction $H_2 \rightarrow 2H^+ + 2e^-$ occurs on the Pt/C electrode, and proton is supplied for the glass-rod continuously. The ionic current was measured using a picoammeter (Keithley 6485). A correction for the secondary electron was not considered in this study.

3. Results and discussion

The obtained glass-rod is porous, and the surface area, pore volume and average pore diameter are estimated to be 434 m^2/g, 0.53 cm^3/g and 4.8 nm, respectively, based on the result of nitrogen gas sorption measurement. Photos of glass-rod after heating at 700°C and that after meniscus-etching are shown in Fig. 3. A smooth taper tip was successfully obtained by using 0.5 % of HF solution. The electric field strength F is proportional to the inverse of the curvature radius r of the tip. The r was estimated to be 60 μm, the electric field strength [V/cm] of which is approximately 160-fold increase as compared with a

flat tip ($r \rightarrow \infty$) at the same voltage [V].

As above mentioned, ion emission current increases with increasing ion conductivity of electrolyte. Nogami *et al.* discussed that proton conduction of the sol-gel-derived porous glasses is promoted by the dissociation of protons from hydroxyl bonds on the pore surfaces and the proton hopping between hydroxyl groups and water molecules. Proton conductivity increases with increasing the content of the adsorbed water [11-14].

Proton conductivity was measured at 30°C under supplying humidified 4%H_2-96%Ar gas (relative humidity 100%). Since the difficulty of the calculation of proton conductivity for such taper-rod shaped sample, finite element method (FEM, COMSOL 5.1 software) was used for the calculation of conductivity. The mesh model and electrical potential [V] are shown in Fig. 4. For the calculation of FEM, conductivity σ was set as fitting parameter and dielectric constant ε was set to 1, and current density i [A/cm^2] at 1 V was calculated. The i was then integrated using the surface area of Ag electrode [cm^2], and resistance R_{FEM} [Ω] was finally obtained using the Ohm's law. Fig. 5a shows cole-cole plots (resistance $R_{\mathrm{experiment}}$) with exposure time for humidified gas. The fitting parameter σ was varied until $R_{\mathrm{FEM}} = R_{\mathrm{experiment}}$. Fig. 5b shows proton conductivity with exposure time. It is important that at least 10 h of exposure time is required to absorb water completely in our setup, and the conductivity reaches higher than 10^{-3} S/cm.

High voltages were applied between the water-absorbed glass-rod and extraction electrode, and ion emission current was measured at room temperature. Figure 6a shows the relationship between the voltage and emission current using the glass-rod shown in Fig. 3. The emission current increases over

~800 V. The same behavior was repeatedly observed. Note that ion emission can be successfully observed at room temperature and non-vacuum atmosphere by utilizing the sol-gel-derived glass-rod. When using a glass-rod without absorption of water, ionic current was not observed, suggesting the ion emission occurs based on the proton conduction. Also, no ionic current was observed in the case for using a glass-rod with flat-edge maybe due to lower electric field strength ($r \to \infty$).

Above ~3 kV, an air discharge occurred, the value is in good agreement with the calculated value using Paschen's law.

$$V_s = \frac{B \cdot p \cdot d}{\ln(A \cdot p \cdot d) - \ln\ln\left(1 + \frac{1}{\gamma}\right)} \qquad (1)$$

where *Vs* is the breakdown voltage, *A* and *B* are constants, *p*, *d*, γ are the pressure, distance between the tip of glass-rod and extraction electrode (here 1 mm), and secondary electron emission coefficient, respectively.

Finally, evidence of the proton emission from the glass-rod is shown based on the protonation reaction of polyaniline. The chemical reaction of polyaniline under a protonation reaction from emeraldine base to eleraldine salt is shown in Fig. 7a. It is known that the color of polyaniline also changes from blue to green by the reaction. Polyaniline (powder) was dispersed in acetone solution and then spin-coated on Si substrate. The substrate was covered with Al foil musk with a hole (3 mm in diameter, Fig. 7b), and ion irradiation was carried out for 12 h at 2.5 kV. The average current was around 0.1 nA, the amount of ion implantation was roughly estimated to be ~1×10^{-11} mol from the current and irradiation time.

At first, Monte Carlo calculation (SRIM software [15]) of the stopping energy of H^+ at 2.5 kV for

aniline is shown in Fig. 8a as a function of penetration depth. If the electron stopping energy at surface (here ~3 eV) is higher than the binding energy of a bond, the bond will cleave. For example, the binding energy of typical single C-H bond is around 4.5 eV, and the acceleration voltage required for breaking this bond can be estimated from the Monte Carlo calculation of stopping energy. The binding energies of polyaniline are C=C (benzene ring, 5.3 eV), C-H (benzene ring, 4.8 eV), C-N (aromatic amine, 4.3 eV), N-H (aromatic amine, 3.4 eV), respectively. It is expected that these all bonds does not cleave at the acceleration voltage (2.5 kV= ~ 3 eV), and only a protonation reaction is considered to occur based on the calculation. Raman spectra of polyaniline films before and after the ion irradiation are shown in Fig. 8b. Characteristic vibrations are seen at 1320 cm^{-1} (stretching vibration of $C\text{-}N^{+}$), 1400 cm^{-1} (stretching vibration of C-C in quinone), 1504 cm^{-1} (stretching vibration of C=N and C=C in quinone), 1560 cm^{-1} (stretching vibration of C=C in quinone) and 1605 cm^{-1} (stretching vibration in phenyl rings) [16,17]. A low intensity band at 1320 cm^{-1} (peak(I)) and strong band at 1504 cm^{-1} are the biggest differences between the spectrum before/after the irradiation. Note that intensity of band of peak(II) decreases and that of peak(I) increases after the irradiation, suggesting the generation of protonated quinones (protonation reaction). We also confirmed the change of film color from blue to green. The ratio of peak intensities, {Intensity of peak(I)} / {Intensity of peak(II)}, and raman mapping is shown in Fig. 8d. Red part of the mapping indicates the higher amount of protonated quinones. Note that protonation reaction occurs selectively on the ion irradiation area. It is evident that proton emission can be seen exactly from the tip of proton conducting glass-rod, and protonation reaction occurs even under non-vacuum atmosphere at room temperature.

In summary, here we report a proton emission at room temperature under non-vacuum atmosphere for the first time by utilizing a proton conducting glass-rod as an emitter. Ionic current was observed only under humidified conditions, and proton conduction is indispensable for our proton emission. Since water molecules also moves accompanying with H^+ owing to an electroosmotic effect, the emitted ions may be not a pure H^+ but H_3O^+ or protonated H_2O cluster. Also, previous ^{31}P MAS NMR measurements revealed that almost all of the PO_4 group is free (Q^0) and there is no chemical bond such as Si-O-P [18], and the stability of the PO_4 group for proton emission should be clarified. Further investigations including mass analysis of the emitted ions as well as a reaction of emitted ions with air are in-progress. Also, proton implantations into body tissues and cells in-air are under studying.

Acknowledgement

This work is supported by JSPS KAKENHI Grant Number 16K14385).

Reference

[1] Roosild S, Dolan R, Buchanan B (1968) J. Electrochem. Soc 115:307-311

[2] Gibbons J. F (1972) Proc. IEEE 60:1062-1096

[3] Wakelin E. A, Fathi A, Kracica M, Yeo, G. C, Wise, S. G, Weiss A. S, McCulloch D. G, Dehghani F, Mckenzie D. R, Bilek M. M. M (2015) ACS Appl Mater Inter 7:23029-23040

[4] Muthukumaran V, Selladurai V, Nandhakumar S, Senthilkumar, M (2010) Mater Des 31:2813-2817

[5] Malka V, Faure J, Gauduel Y. A, Lefebvre E, Rousse A, Phuoc K. T (2008) Nat Phys 4:447-453

[6] Torimoto Y, Harano A, Suda T, Sadakata M (1997) Jpn J Appl Phys 36:L238-240

[7] Fujiwara Y, Kaimai A, Hong J.-O, Yashiro K, Nigara Y, Kawada T, Mizusaki J (2003) J Electrochem Soc 150:E117-124

[8] Li Q, Hosono H, Hirano M, Hayashi K, Nishioka M, Kashiwagi H, Torimoto Y, Sadakata M (2003) Sur. Sci 527:100-112

[9] Li J, Hayashi K, Hirano M, Hosono H (2009) Solid State Ionics 180:1113-1117

[10] Daiko Y (2016) Proc. IEEE 16th Int. Conf. Nanotechnology 351 (DOI: 10.1109/NANO.2016.7751521)

[11] Nogami M, Daiko Y, Akai T, Kasuga T (2001) J. Phys. Chem. B 105:4653-4656

[12] Daiko Y, Kasuga T, Nogami M (2002) Chem. Mater 14:4624-4627

[13] Daiko Y (2014) J. Sol-Gel Sci. Technol 70:172-179

[14] Nogami M (1998) J. Phys. Chem. B 102:5772-5775

[15] Biersack J. P, Haggmark L (1980) Nucl. Instr. Meth 174:257-269

[16] Grzeszczuk M, Grańska. Roman Szostak (2013) Int J Electrochem Sci 8:8951-8965

[17] Zhang J, Liu C, Shi G (2005) J Appl Poly Sci 96:732-739

[18] Nogami M, Goto Y, Kasuga T (2003) J Am Ceram Soc 86:1504-1507

Figure captions

Figure 1 Schematic illustration of meniscus-etching method.

Figure 2 Experimental setup for H^+ conductivity and H^+ emission measurements (1: glass-rod, 2: Ag paste electrode, 3: LCR meter, 4: Pt/C electrode, 5: Al plate with a hole (3.5 mm) as an extraction electrode, 6: high voltage DC power supply, 7: target plate (Al), 8: picoammeter).

Figure 3 (left) Photos of glass-rod after heating at 700°C, (left) enlarged picture by optical microscope of the tip of the glass-rod after meniscus-etching treatment.

Figure 4 Mesh model and electrical potential distribution of glass-rod for FEM calculation of conductivity. The number of elements used was 87,000.

Figure 5 (a) Cole-Cole plots and (b) proton conductivity as a function of exposure time to humidified 4%H_2-96%Ar gas measured at 30°C.

Figure 6 Relationship between the acceleration voltage and ion emission currents for (a) sharp-edge and (b) flat-shape glass-rod.

Figure 7 (a) Structures of polyaniline (emeraldine base and emeraldine salt), (b) experimental setup of H+ emission for polyaniline, and (b) the ion emission current at 2.5 kV with time.

Figure 8 (a) Monte Carlo calculation of the stopping energy for H^+ at 2.5 kV for anilinem (b) raman spectra of polyaniline before [black line] and after [red line] ion irradiation for 12 h, (c) raman spectrum with fitting curves and (d) raman mapping for the intensity ratio of peak(I) / peak(II).

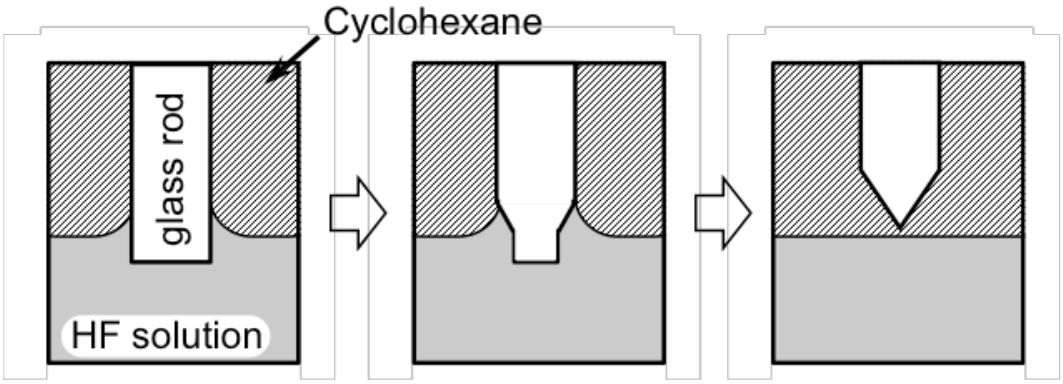

Fig. 1
Schematic illustration of meniscus-etching method.

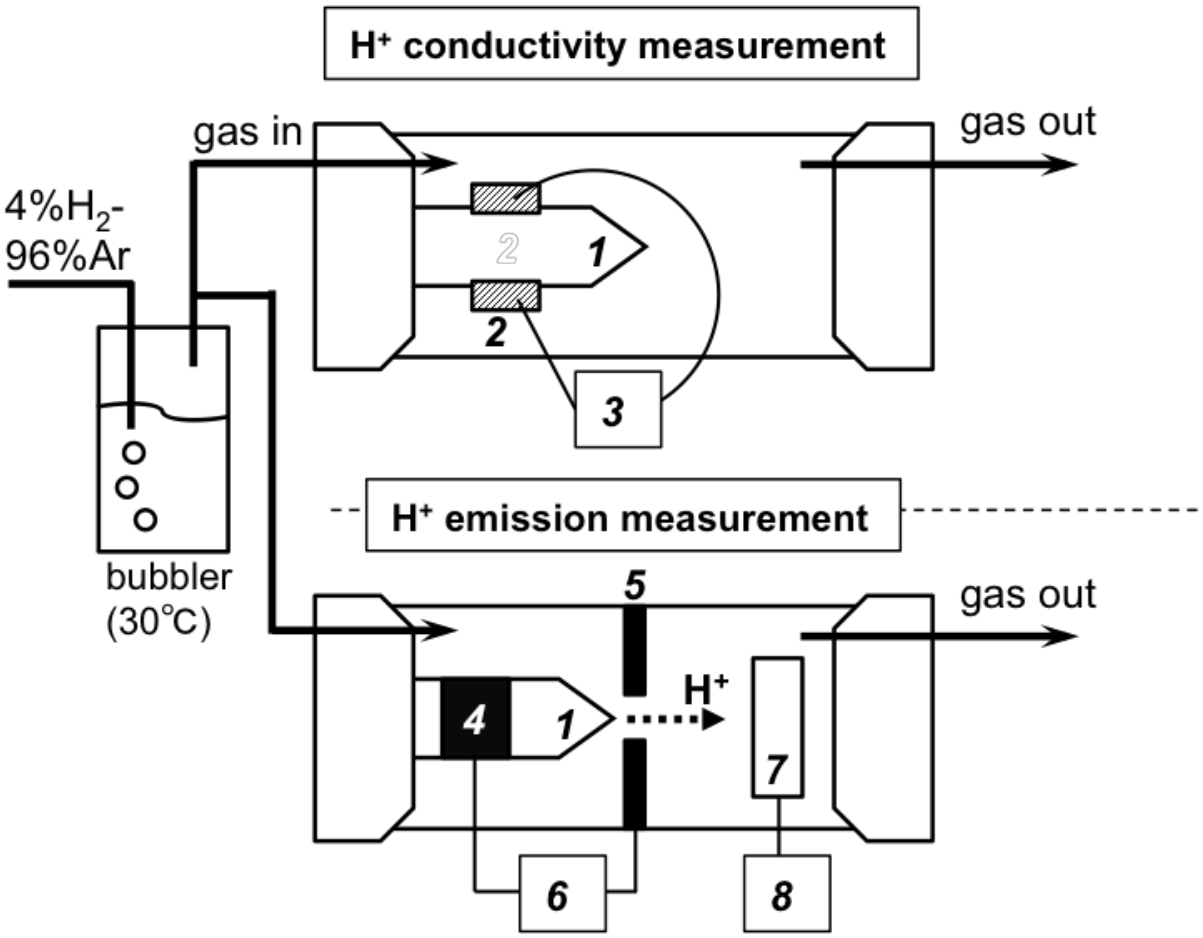

Figure 2

Experimental setup for H^+ conductivity and H^+ emission measurements (1: glass-rod, 2: Ag paste electrode, 3: LCR meter, 4: Pt/C electrode, 5: Al plate with a hole (3.5 mm) as an extraction electrode, 6: high voltage DC power supply, 7: target plate (Al), 8: picoammeter).

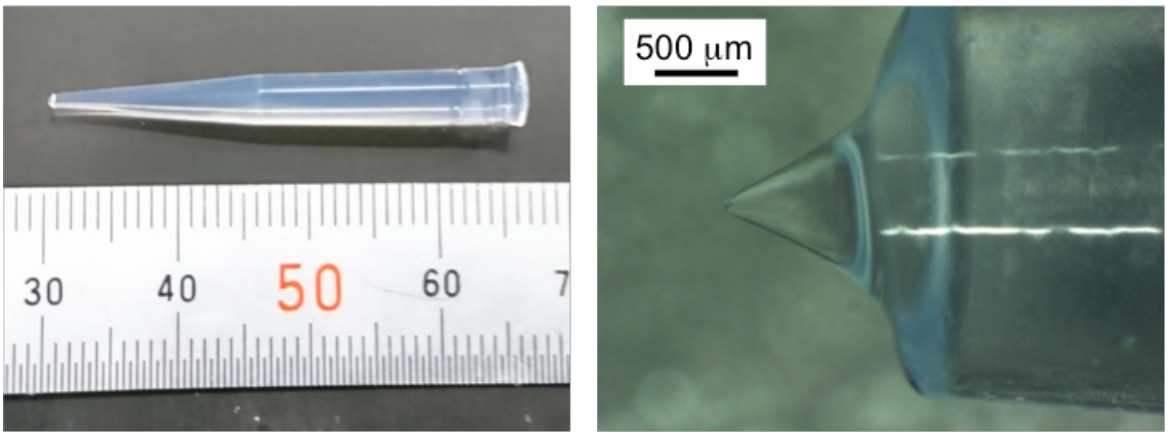

Figure 3
(left) Photos of glass-rod after heating at 700°C, (left) enlarged picture by optical microscope of the tip of the glass-rod after meniscus-etching treatment.

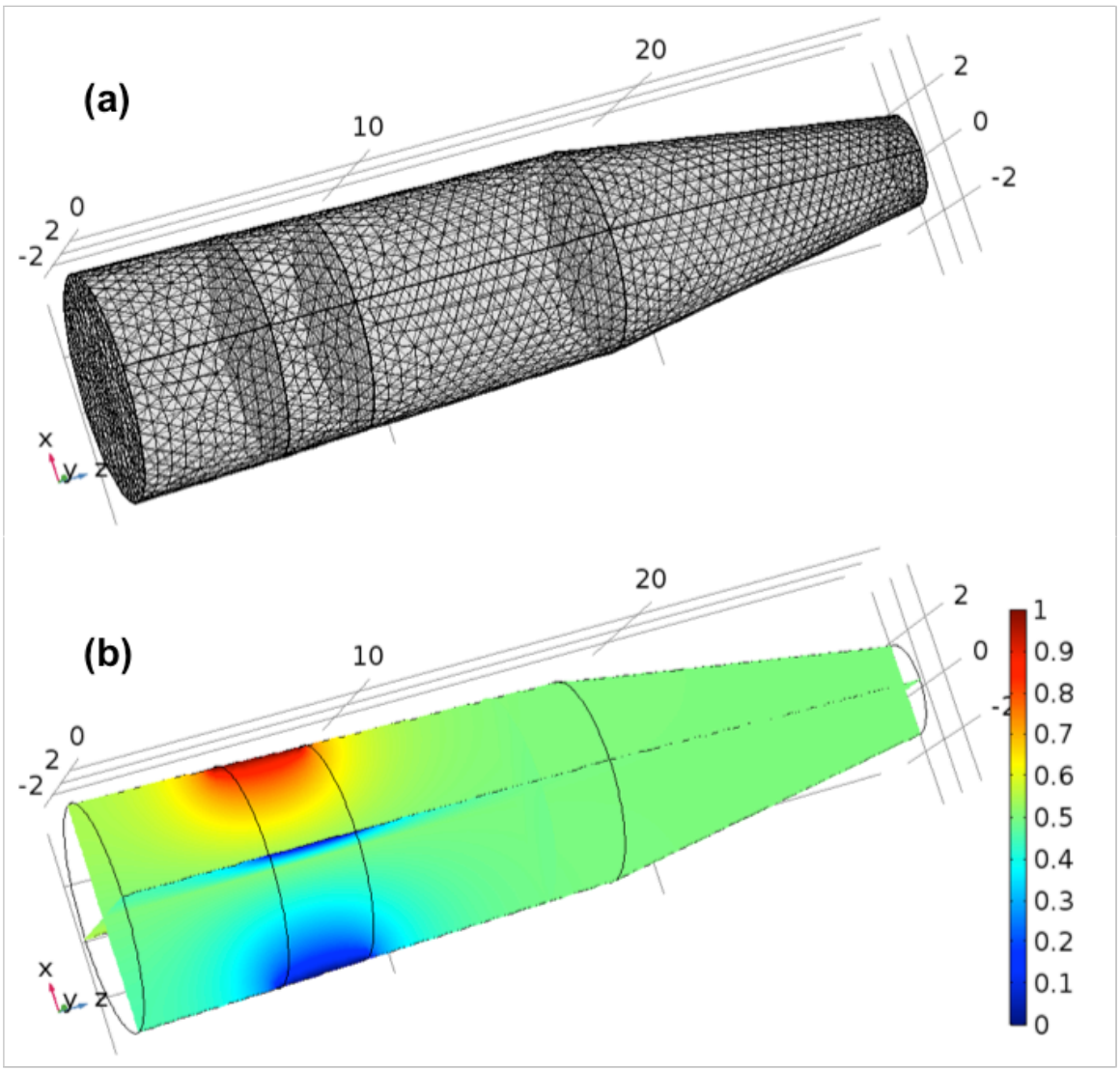

Figure 4
Mesh model and electrical potential distribution of glass-rod for FEM calculation of conductivity. The number of elements used was 87,000.

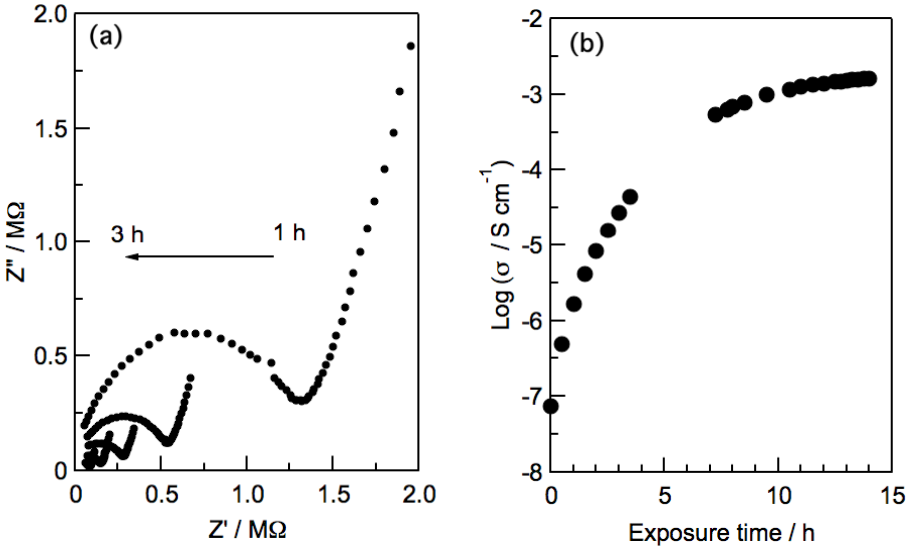

Figure 5

(a) Cole-Cole plots and (b) proton conductivity as a function of exposure time to humidified 4%H_2-96%Ar gas measured at 30°C.

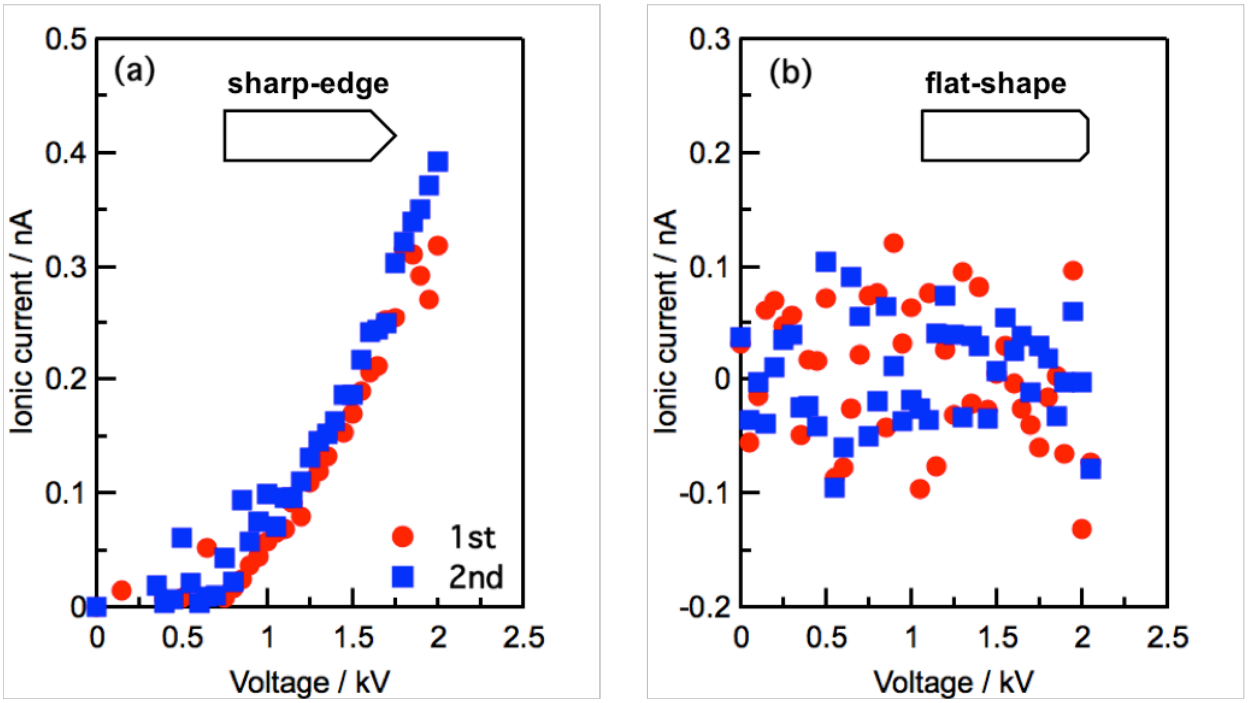

Figure 6

Relationship between the acceleration voltage and ion emission currents for (a) sharp-edge and (b) flat-shape glass-rod.

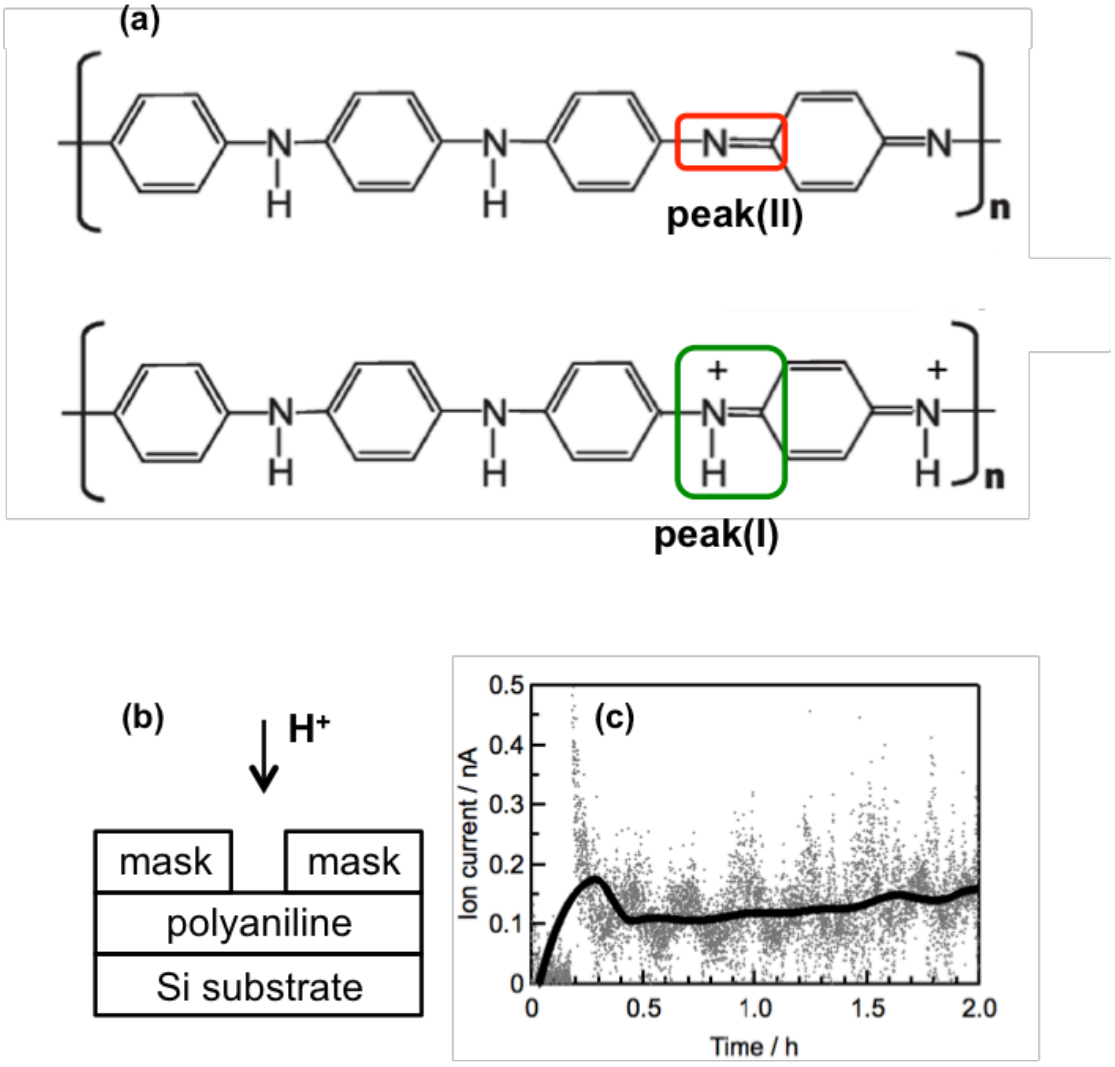

Figure 7

(a) Structures of polyaniline (emeraldine base and emeraldine salt), (b) experimental setup of H+ emission for polyaniline, and (b) the ion emission current at 2.5 kV with time

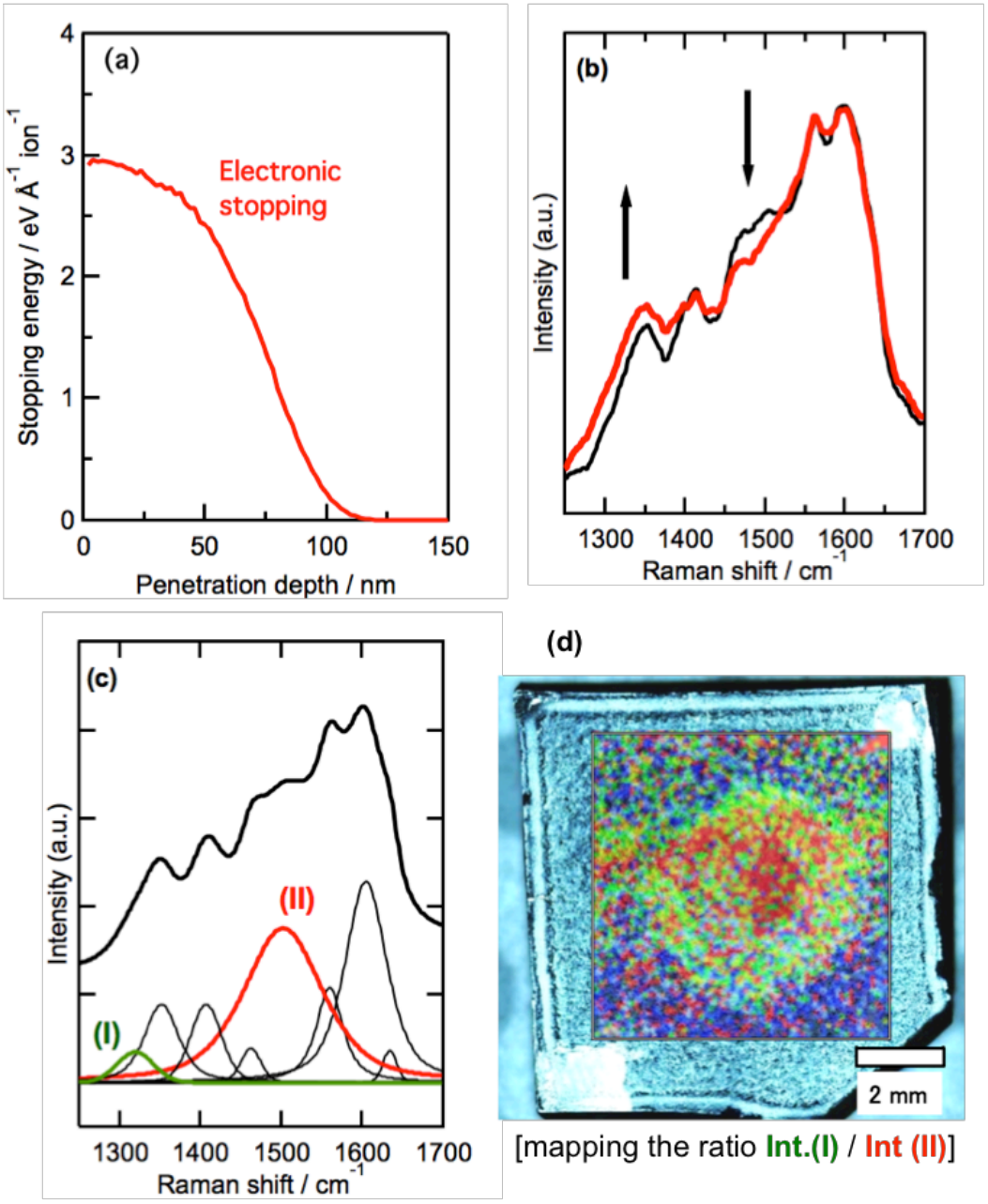

Figure 8

(a) Monte Carlo calculation of the stopping energy for H^+ at 2.5 kV for anilinem (b) raman spectra of polyaniline before [black line] and after [red line] ion irradiation for 12 h, (c) raman spectrum with fitting curves and (d) raman mapping for the intensity ratio of peak(I) / peak(II).